On the complexity of the 1,3-dithiole-2-thione chromophore

UV-Vis polarization spectroscopy and theoretical calculations

Visby, Kristin; Spanget-Larsen, Jens

Published in:
Chemical Physics

DOI:
10.1016/j.chemphys.2022.111574

Publication date:
2022

Document Version
Publisher's PDF, also known as Version of record

Citation for published version (APA):
Visby, K., & Spanget-Larsen, J. (2022). On the complexity of the 1,3-dithiole-2-thione chromophore: UV-Vis polarization spectroscopy and theoretical calculations. *Chemical Physics*, *560*(2-3), Article 111574. https://doi.org/10.1016/j.chemphys.2022.111574

Chemical Physics 560 (2022) 111574

Contents lists available at ScienceDirect

Chemical Physics

journal homepage: www.elsevier.com/locate/chemphys

On the complexity of the 1,3-dithiole-2-thione chromophore. UV-Vis polarization spectroscopy and theoretical calculations

Kristin Visby [1], Jens Spanget-Larsen [*]

Dept. of Science and Environment, Roskilde University, P.O.Box 260, DK-4000 Roskilde, Denmark

ARTICLE INFO

Keywords:
Linear Dichroism (LD)
Polarization spectroscopy
Electronic transitions
UV-Vis spectroscopy
Time-Dependent Density Functional Theory (TD-DFT)
Diffuse basis functions

ABSTRACT

The electronic transitions of 1,3-dithiole-2-thione (DTT) are investigated by Linear Dichroism (LD) spectroscopy in the near-UV and visible regions and by quantum chemical calculations. The LD experiments are performed in the spectral region 46,000–20,000 cm^{-1} (217 - 500 nm) using stretched polyethylene (PE) as an anisotropic solvent. The observed spectral features are compared with electronic transitions calculated by Time-Dependent Density Functional Theory (TD-DFT) considering different functionals and a variety of basis sets. The DTT chromophore is complex and a full elucidation may require the application of more advanced theoretical models with consideration of multiply excited electronic configurations and evaluation of multi-state vibronic couplings.

1. Introduction

Thulstrup et al. [1] recently investigated the electronic transitions of tetrathiafulvalene (TTF, Scheme 1) by Linear Dichroism (LD) polarization spectroscopy and theoretical calculations, leading to a reinterpretation of several features of the UV absorption spectrum of TTF. This has prompted us to perform a similar investigation of the related compound 1,3-dithiole-2-thione (DTT, Scheme 1), the starting material in the TTF synthesis [2].

Gleiter et al. [3] performed a detailed study of the electronic structure of DTT and several related species by photoelectron spectroscopy and electronic absorption spectroscopy. The electronic transitions were investigated by LD polarization spectroscopy in the near-UV region on samples aligned in stretched polyethylene (PE) at 77 K. The spectra were analyzed in terms of partial absorbance curves [4–8] and the main bands were assigned to electronic transitions predicted by semiempirical Pariser-Parr-Pople (PPP) [9–11] π-electron calculations. However, the results for DTT were incomplete. The determination of one of the partial absorbance curves was tentative, and the authors found that a detailed understanding of the excited states required "a more sophisticated theoretical treatment", probably with inclusion of "4s and 3d on sulfur". They felt that the presented polarization spectra for DTT "might serve as a useful test of such a treatment" [3]. But to the best of our knowledge, the results of more advanced treatments like the one suggested by Gleiter et al. have not yet been published.

In this publication we present the results of an experimental and theoretical investigation of the electronic transitions of DTT. We have remeasured the LD spectra in the near-UV and visible regions of molecular samples aligned in stretched PE. To support the analysis in terms of partial absorbance curves, we have recorded corresponding LD spectra in the IR region, allowing independent determination of all three orientation factors [4–8] (Section 4.1). As we shall show, the results lead to partial revision of the previously published near-UV spectrum of DTT [3]. The observed absorption bands are discussed with reference to transitions calculated with Time-Dependent Density Functional Theory (TD-DFT) [12–14]. The calculations were performed with large, multiple-zeta basis sets, including polarization and diffuse functions. This level of theory led to excellent prediction of the observed near-UV spectra of TTF [1]. Additional information is provided as Supplementary data, referred to in the ensuing text as S1–S9.

2. Experimental

2.1. Materials

1,3-Dithiole-3-thione (DTT) [CAS 930-35-8] (98%) was purchased as a yellow solid from Sigma-Aldrich (vinylene trithiocarbonate, cat. no. 358916). The spectroscopic purity of the substance was checked by comparison with literature spectra [15–17]. Low-density polyethylene (PE) was obtained as pure sheet material from Hinnum Plast, DK-2670

* Corresponding author.
E-mail address: spanget@ruc.dk (J. Spanget-Larsen).
[1] Present affiliation: Radiometer Medical ApS, Denmark.

https://doi.org/10.1016/j.chemphys.2022.111574
Received 23 February 2022; Received in revised form 11 April 2022; Accepted 28 April 2022
Available online 4 May 2022

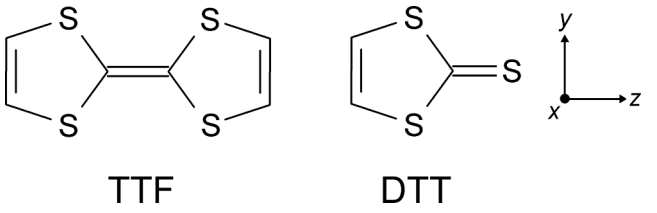

Scheme 1. Tetrathiafulvalene (TTF) and 1,3-dithiole-2-thione (DTT) with indication of the applied coordinate system.

Greve, Denmark. Methanol was spectroscopic grade (Uvasol) from Sigma-Aldrich.

2.2. Sample preparation

DTT was introduced into the PE material by sublimation at 31 °C for one to three days. For recording of the absorption in the UV region, a single sheet of 50 μm thickness was applied. For the visible and IR regions, a thick PE sample was produced by uniting 20 pieces of 100 μm sheet material through a procedure of heating and pressing. The surfaces of the samples were subsequently cleaned with methanol to remove crystalline deposits. Similar samples were produced without introduction of DTT for use as references. Polarization spectroscopic absorbance measurements were performed on samples uniaxially stretched by ca. 500%. Further information on stretched PE samples can be found in the literature [4–8].

2.3. Linear Dichroism measurements

UV-Vis and IR Linear Dichroism (LD) polarization spectra were measured at room temperature as previously described [6]. The UV-Vis spectra were recorded in the region 46,000–20,000 cm^{-1} (217–500 nm) with a slit width of 1 nm on a Shimadzu MPS-2000 spectrophotometer with a rotatable Glan prism polarizer in the sample beam. The IR LD spectra were recorded in the region 4,000–400 cm^{-1} as the average of 100 scans with a resolution of 2 cm^{-1} on a Perkin-Elmer Model 1710 FTIR spectrophotometer equipped with a SPECAC Model KRS-5 polarizer. The baseline-corrected LD absorbance curves are denoted $E_U(\tilde{\nu})$ and $E_V(\tilde{\nu})$, corresponding to absorption polarized parallel and perpendicular to the uniaxial stretching direction U of the polymer. The resulting UV-Vis LD curves are shown in Fig. 1 (top), and observed UV-Vis absorbance peaks are listed in Table 1. The IR LD spectra are provided as Supplementary data S1.

3. Theoretical calculations

Quantum chemical calculations on DTT in the gas phase were performed with the Gaussian 16 [18] software package. The molecular ground state equilibrium C_{2v} geometry was computed with the long range-corrected density functional CAM-B3LYP [19]. Vertical electronic transitions to excited singlet states were computed with TD–CAM-B3LYP. This procedure was recently successful in prediction of the electronic transitions of TTF [1]. A constant value of 4500 cm^{-1} was subtracted from the excitation wavenumbers computed with TD–CAM-B3LYP to facilitate comparison of observed and predicted trends [20–23]. Oscillator strengths were evaluated from the computed ground to excited state transition electric dipole moments by using the dipole length formulation [14,18]. To investigate the basis set dependence of the predicted transitions, the calculations were performed with several basis sets: 6-311++G(3df,3pd) [14,18], cc-pVTZ, AUG-cc-pVTZ, AUG-cc-pVQZ, and AUG-cc-pV5Z [18,24,25]. Additional calculations were performed using the long-range corrected functionals LC-ωPBE [26,27] and ωB97XD [28] with the basis AUG-cc-pVTZ. Graphical convolutions of the predicted transitions were performed by assigning a Gaussian function to each excitation wavenumber with an area proportional to the oscillator strength of that transition, using a constant standard deviation, σ = 1500 cm^{-1} (2.355 σ ≈ Full Width at Half Maximum (FWHM)). Nuclear coordinates, predicted transitions, and graphical representations are provided in S2–S9. Direct comparisons of transitions predicted with and without diffuse functions in the basis set are provided in S7. Transitions predicted with TD–CAM-B3LYP/AUG-cc-pVTZ are listed in Table 1 and visualized in Fig. 2 (bottom). The molecular orbital (MO) surface diagrams shown in Figs. 3 and S4 were computed with CAM-B3LYP/AUG-cc-pVTZ and visualized using GaussView 6 [29] with a constant isovalue equal to 0.02.

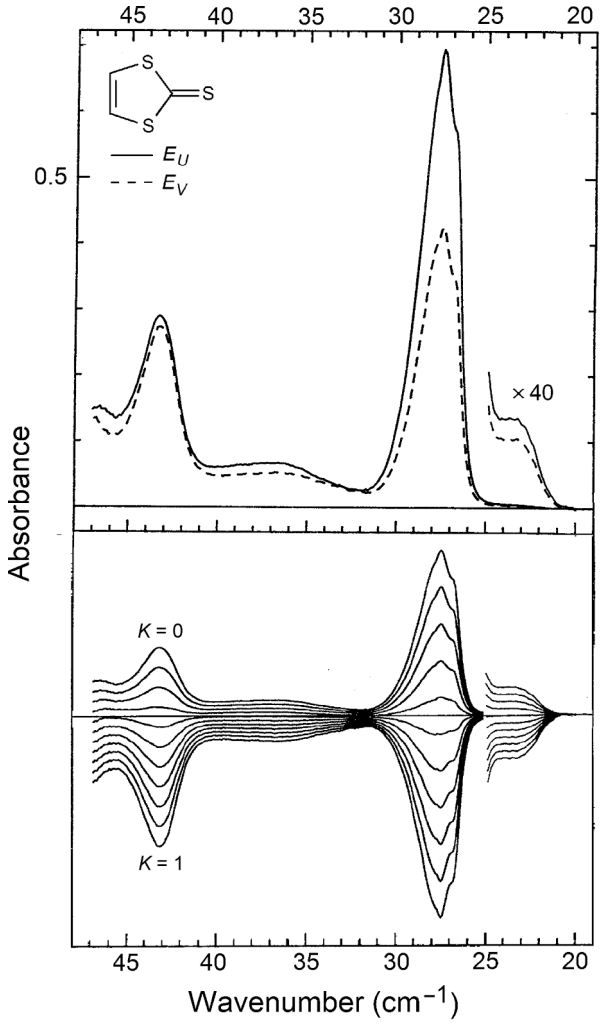

Fig. 1. *Top:* Linear Dichroic (LD) absorbance curves recorded for DTT partially aligned in stretched polyethylene (PE) at room temperature. The inserted curves in the visible region were recorded using a thick PE sample (Section 2.2). $E_U(\tilde{\nu})$ and $E_V(\tilde{\nu})$ denote absorbance measured with radiation polarized parallel and perpendicular to the stretching axis U of the sample. *Bottom:* Linear combinations $r_K(\tilde{\nu}) = (1-K)E_U(\tilde{\nu}) - 2KE_V(\tilde{\nu})$ with K ranging from 0 to 1 in steps of 0.1, allowing assignment of K-values (Section 4.1).

4. Results and discussion

4.1. Linear Dichroism (LD): orientation factors and partial absorbance curves

The observed LD absorbance curves $E_U(\tilde{\nu})$ and $E_V(\tilde{\nu})$ for DTT partially aligned in stretched PE are shown in Fig. 1 (top). The directional information that can be derived from the LD curves is given by the orientation factors K_i [4–8]:

Table 1
Observed features of the LD spectrum of 1,3-dithiole-2-thione (DTT) and calculated electronic transitions.

Observed				TD–CAM-B3LYP/AUG-cc-pVTZ [a]			
	$\tilde{\nu}$ [b]	Log ε [c]	Pol [d]	Term	$\tilde{\nu}$ [b,e]	f [f]	Leading configurations [g]
A	22.3	1.9	*z*	$1\ ^1A_2$ (-)	19.0	0	99% [$11b_2 \rightarrow 6b_1$]
B	27.2	4.2	*z*	$2\ ^1A_1$ (*z*)	26.7	**0.180**	97% [$5b_1 \rightarrow 6b_1$]
				$1\ ^1B_1$ (*x*)	32.5	0.001	83% [$5b_1 \rightarrow 18a_1$]; 11% [$5b_1 \rightarrow 17a_1$]
C [h]	35	3.0	*x,y*	$1\ ^1B_2$ (*y*)	35.6	**0.022**	91% [$5b_1 \rightarrow 3a_2$]
				$2\ ^1B_2$ (*y*)	38.1	0.005	81% [$11b_2 \rightarrow 18a_1$]
D [i]	37.4	3.2	*z*	$2\ ^1B_1$ (*x*)	39.7	$7{\cdot}10^{-4}$	74% [$5b_1 \rightarrow 17a_1$]; 10% [$5b_1 \rightarrow 18a_1$]
				$3\ ^1B_1$ (*x*)	40.5	0.002	98% [$11b_2 \rightarrow 3a_2$]
				$2\ ^1A_2$ (-)	42.1	0	39% [$5b_1 \rightarrow 12b_2$]; 23% [$5b_1 \rightarrow 14b_2$]
				$3\ ^1B_2$ (*y*)	43.4	0.015	58% [$2a_2 \rightarrow 6b_1$]; 22% [$11b_2 \rightarrow 19a_1$]
				$4\ ^1B_1$ (*x*)	43.7	$1{\cdot}10^{-4}$	83% [$5b_1 \rightarrow 19a_1$]
E	43.0	3.9	*x,y*	$4\ ^1B_2$ (*y*)	44.7	**0.108**	47% [$11b_2 \rightarrow 17a_1$]; 21% [$2a_2 \rightarrow 6b_1$]
				$5\ ^1B_2$ (*y*)	46.5	**0.065**	32% [$11b_2 \rightarrow 20a_1$]; 31% [$11b_2 \rightarrow 19a_1$]
				$3\ ^1A_2$ (-)	47.2	0	51% [$5b_1 \rightarrow 12b_2$]; 23% [$5b_1 \rightarrow 13b_2$]
				$5\ ^1B_1$ (*x*)	47.2	$2{\cdot}10^{-4}$	65% [$5b_1 \rightarrow 21a_1$]; 20% [$5b_1 \rightarrow 20a_1$]
				$3\ ^1A_1$ (*z*)	47.7	$1{\cdot}10^{-4}$	68% [$4b_1 \rightarrow 6b_1$]; 10% [$11b_2 \rightarrow 14b_2$]
				$4\ ^1A_1$ (*z*)	48.5	**0.087**	30% [$11b_2 \rightarrow 12b_2$]; 23% [$11b_2 \rightarrow 13b_2$]
				$4\ ^1A_2$ (-)	49.5	0	57% [$10b_2 \rightarrow 6b_1$]; 14% [$2a_2 \rightarrow 18a_1$]
				$5\ ^1A_1$ (*z*)	50.0	**0.049**	88% [$5b_1 \rightarrow 7b_1$]

[a] 18 lowest transitions. Full listing provided as S4.
[b] Peak wavenumber in 1000 cm^{-1}.
[c] Cyclohexane solution [3].
[d] Polarization direction, see main text.
[e] 4500 cm^{-1} subtracted from the calculated wavenumbers.
[f] Oscillator strength.
[g] Some important MOs are shown in Fig. 3.
[h] Very broad band.
[i] Assignment of this band is problematic, see Section 4.2.

$$K_i = \langle \cos^2\left(\vec{M}_i, U\right)\rangle \tag{1}$$

$\left(\vec{M}_i, U\right)$ is the angle of the electric dipole moment vector $\vec{M}_i$ of transition *i* with the uniaxial stretching direction *U* of the polymer, and the pointed brackets indicate the average over all solute molecules in the light path. The K_i values may be determined by the graphical TEM (Trial and Error Method) procedure [4–6] which involves formation of linear combinations of $E_U(\tilde{\nu})$ and $E_V(\tilde{\nu})$. We consider the reduced absorbance curves $r_K(\tilde{\nu})$ [6]:

$$r_K(\tilde{\nu}) = (1-K)E_U(\tilde{\nu}) - 2KE_V(\tilde{\nu}) \tag{2}$$

A family of curves $r_K(\tilde{\nu})$ for DTT is shown in Fig. 1 (bottom). A spectral feature due to transition *i* vanishes from the linear combination $r_K(\tilde{\nu})$ for $K = K_i$ and the K_i value may be determined by visual inspection [6]. In the present case of molecular C_{2v} symmetry, optically allowed transitions must be polarized along the three symmetry axes *x*, *y*, and *z* (Scheme 1), corresponding to transitions to excited states of B_1, B_2, and A_1 symmetry. Hence, we should observe only three different K_i values equal to K_x, K_y and K_z, the orientation factors of the three molecular axes, and the three values should add up to unity, $K_x + K_y + K_z = 1$.

The IR polarization spectra of DTT aligned in a thick, stretched PE sample provides a direct determination of all three *K* values: $(K_x, K_y, K_z) = (0.27 \pm 0.01, 0.33 \pm 0.01, 0.41 \pm 0.01)$, see Supplementary data S1. Inspection of the family of reduced UV-Vis curves in Fig. 1 (bottom) obtained from measurements in a thin sheet of PE leads to $K = 0.45$ for the intense feature at 27,200 cm^{-1} and $K = 0.34$ for the one at 43,000 cm^{-1}. These values must be assigned to K_z and K_y, corresponding to in-plane long and short axis-polarized transitions, respectively. We thus have $(K_x, K_y, K_z) = (0.21, 0.34, 0.45)$, where K_x is obtained from $K_x = 1 - K_y - K_z$. These values are consistent with those determined in the IR spectroscopic experiment (S1), indicating slightly improved alignment in the thin sample.

Gleiter et al. [3] determined the dichroic ratios $d_y = 0.8$ and $d_z = 1/0.61 = 1.64$ for DTT aligned in stretched PE. These dichroic ratios correspond to the orientation factors $K_y = d_y/(1+d_y) = 0.29$ and $K_z = d_z/(1+d_z) = 0.45$. The latter value is equal to the one obtained in the present study, but $K_y = 0.29$ seems to disagree with the present value $K_y = 0.34$. But the authors stated that their value of d_y was "not well determined" because of "the apparent absence of a strong purely *y*-polarized peak" [3]. As indicated above, $K_y = 0.34$ is supported by IR LD spectroscopy, leading to $K_y = 0.33 \pm 0.01$ (S1).

Following Madsen et al. [6] we construct the pair of reduced absorbance curves $E_{-z}(\tilde{\nu})$ and $E_{-y}(\tilde{\nu})$:

$$E_{-z}(\tilde{\nu}) = \left(K_y - K_z\right)^{-1} r_{K_z}(\tilde{\nu}) \qquad E_{-y}(\tilde{\nu}) = \left(K_z - K_y\right)^{-1} r_{K_y}(\tilde{\nu}) \tag{3}$$

Contributions from *z*-polarized transitions are absent in $E_{-z}(\tilde{\nu})$ and those of *y*-polarized transitions are absent in $E_{-y}(\tilde{\nu})$. The resulting curves produced with $(K_y, K_z) = (0.34, 0.45)$ are shown in Fig. 2 (top). They are related to the partial absorbance curves $A_x(\tilde{\nu})$, $A_y(\tilde{\nu})$, and $A_z(\tilde{\nu})$, corresponding to absorbance polarized along the three symmetry axes of the molecule, through expressions derived by Madsen et al. [6]. With $(K_x, K_y, K_z) = (0.21, 0.34, 0.45)$ we obtain:

$$\begin{aligned} E_{-z}(\tilde{\nu}) &= A_y(\tilde{\nu}) + \frac{K_x - K_z}{K_y - K_z}A_x(\tilde{\nu}) = A_y(\tilde{\nu}) + 2.2\,A_x(\tilde{\nu}) \\ E_{-y}(\tilde{\nu}) &= A_z(\tilde{\nu}) + \frac{K_x - K_y}{K_z - K_y}A_x(\tilde{\nu}) = A_z(\tilde{\nu}) - 1.2\,A_x(\tilde{\nu}) \end{aligned} \tag{4}$$

4.2. Electronic transitions

As indicated in Eqns. (4), the reduced absorbance curves $E_{-z}(\tilde{\nu})$ and $E_{-y}(\tilde{\nu})$ shown in Fig. 2 (top) contain linear combinations of the partial absorbance curves $A_x(\tilde{\nu})$, $A_y(\tilde{\nu})$, and $A_z(\tilde{\nu})$. For simplicity, we shall in the following refer to $E_{-z}(\tilde{\nu})$ and $E_{-y}(\tilde{\nu})$ as short axis- and long axis-polarized absorbance curves, respectively. Fig. 2 (bottom) shows the transitions predicted with TD–CAM-B3LYP/AUG-cc-pVTZ, as well as Gaussian convolutions constructed to correspond to the reduced absorbance curves $E_{-z}(\tilde{\nu})$ and $E_{-y}(\tilde{\nu})$ according to Eqns. (4). The observed spectral features *A*, *B*, *C*, *D*, and *E* and the suggested assignments to calculated

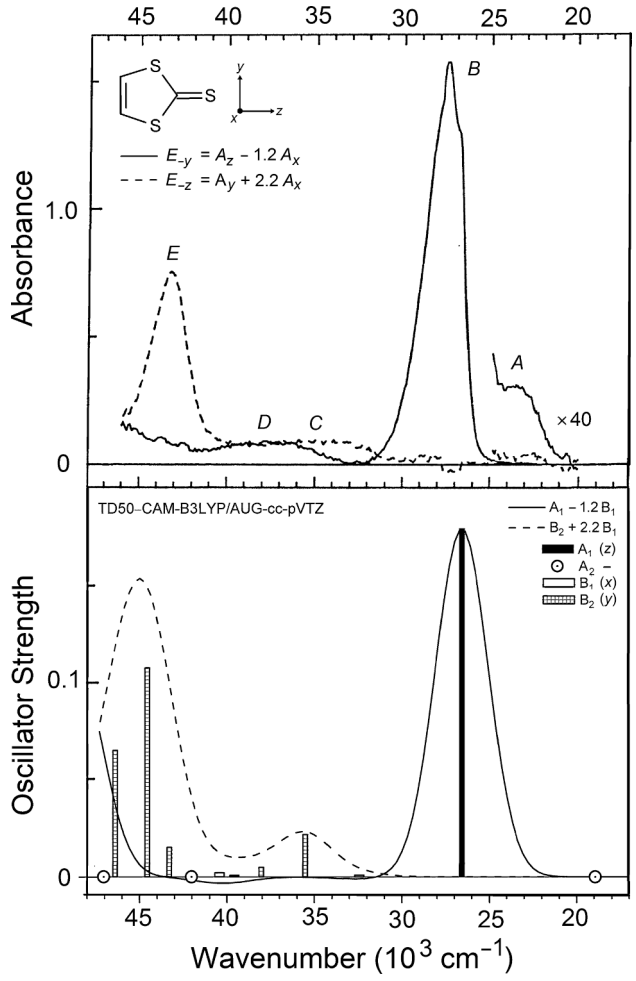

Fig. 2. *Top:* Reduced absorbance curves $E_{-y}(\tilde{\nu}) = A_z(\tilde{\nu}) - 1.2\,A_x(\tilde{\nu})$ and $E_{-z}(\tilde{\nu}) = A_y(\tilde{\nu}) + 2.2\,A_x(\tilde{\nu})$ derived from the observed LD absorbance curves $E_U(\tilde{\nu})$ and $E_V(\tilde{\nu})$ according to Eqns. (3) and (4). *Bottom:* Graphical representation of electronic transitions predicted with TD–CAM-B3LYP/AUG-cc-pVTZ (Table 1). The Gaussian convolutions indicate linear combinations corresponding to the reduced absorbance curves $E_{-y}(\tilde{\nu})$ and$E_{-z}(\tilde{\nu})$.

electronic transitions are listed in Table 1.

The LD absorbance curves recorded at low temperature (77 K) by Gleiter et al. [3] are similar to those shown in Fig. 2 (top), except for the presence of an additional, long axis-polarized band *F* with a maximum at 43,600 cm^{-1} (229 nm). This band was tentatively assigned to a separate electronic transition [3], but it is neither observed nor predicted in the present study. The appearance of this feature in the previously published spectrum is probably due to incomplete reduction (see the discussion in Section 4.1).

The visible region displays a very weak band *A*, overlapping the foot of the much stronger transition *B*. Band *A* has an apparent onset around 20,000 cm^{-1} (500 nm) and a maximum at 22,300 cm^{-1} (448 nm). It can probably be assigned to the optically forbidden state $1\,^1A_2$ predicted at 19,000 cm^{-1} (526 nm) (Table 1). This is an *n*-π^* state corresponding to promotion of an electron from $11b_2(n)$ to $6b_1(\pi^*)$ (Fig. 3). The possible assignment of an *n*-π^* transition is supported by the observed low intensity and negative solvatochromism and agrees with previous suggestions [3,15]. Band *A* is long axis-polarized, but the observed polarization of this very weak absorbance can probably be explained by intensity borrowed from the strong, *z*-polarized band *B* by vibronic coupling [30–33].

The absorbance in the near-UV region is dominated by two differently polarized, prominent features *B* and *E* at 27,200 and 43,000 cm^{-1}

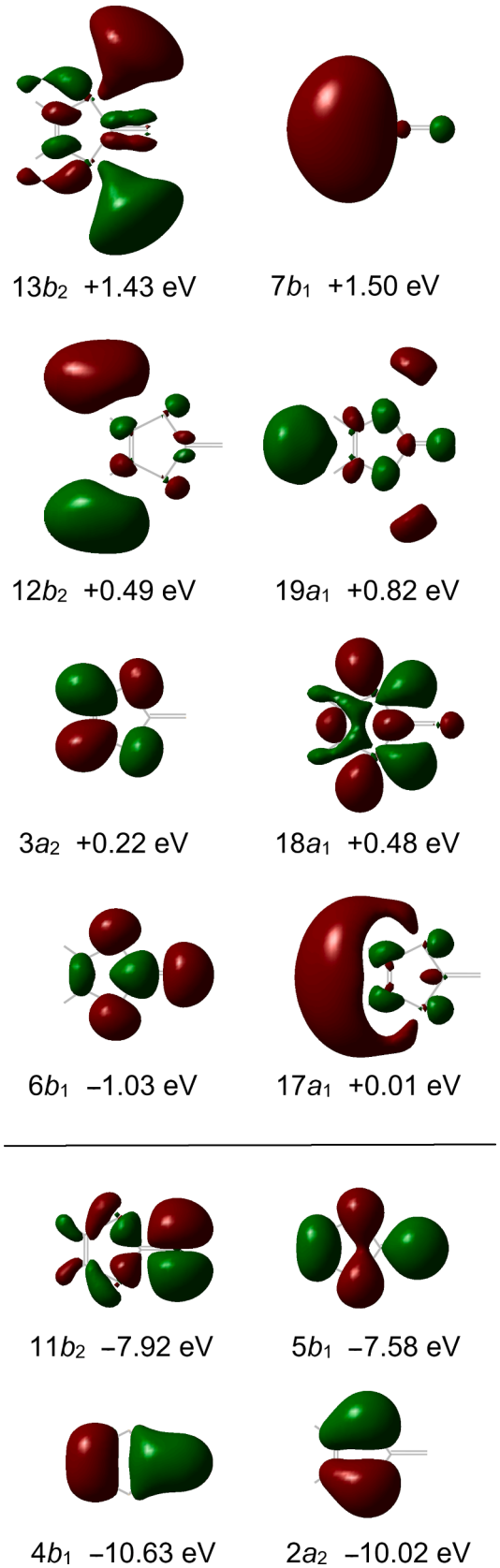

Fig. 3. Symmetry and energy (eV) of the four highest occupied and six lowest unoccupied molecular orbitals (MOs) computed with CAM-B3LYP/AUG-cc-pVTZ with indication of the orbital shape.

(368 and 233 nm). Band *B* is long axis-polarized and is easily assigned to the strong, *z*-polarized transition to the state 2 $^1A_1$ predicted at 26,700 cm^{-1} (375 nm). This transition is well described by the promotion $5b_1(\pi) \rightarrow 6b_1(\pi^*)$. Transition *E* is short axis-polarized and can be assigned primarily to the strong, *y*-polarized transition to the 4 $^1B_2$ state computed at 44,700 cm^{-1} (224 nm), with additional contributions from transitions to 3 $^1B_2$ and 5 $^1B_2$ computed at 43,400 and 46,500 cm^{-1} (230 and 215 nm). These three $^1B_2$ states are predicted to involve relatively diffuse virtual MOs characterized by admixture of valence and Rydberg character, such as $17a_1$ and $19a_1$ (Fig. 3). In the absence of diffuse functions in the basis set, a single intense $^1B_2$ state is predicted, namely 3 $^1B_2$ at 44,800 cm^{-1} dominated by the promotion $2a_2(\pi) \rightarrow 6b_1(\pi^*)$ (S3, S7).

Gleiter et al. [3] assigned bands *B* and *E* to π-π* transitions predicted by PPP calculations. The assignments were supported by correlation with transitions observed for three selenium analogues of DTT and seem well-established. On the other hand, the results of the present calculations suggest that band *B* may be of a composite nature and may involve excitations of other than π-π* type.

The spectral region between the two major bands *B* and *E* is characterized by weak and overlapping contributions. Assignment to the numerous transitions predicted in this region is not straightforward. The number of predicted transitions depends on the inclusion of diffuse functions in the basis set (S7). At least half a dozen transitions are computed in this region with TD–CAM-B3LYP/AUG-cc-pVTZ (Table 1).

The short axis-polarized absorbance band *C* has almost constant intensity from 32,000 to 40,000 cm^{-1} (313 to 250 nm), overlapping the onset of band *E*. This absorbance can be assigned primarily to the 1 $^1B_2$ state computed at 35,600 cm^{-1} (281 nm) with a minor contribution from the 2 $^1B_2$ state predicted at 38,100 cm^{-1} (262 nm), both giving rise to *y*-polarized intensity. The two states are described by the leading promotions $5b_1(\pi) \rightarrow 3a_2(\pi^*)$ and $11b_2(n) \rightarrow 18a_1(\sigma^*)$, respectively. Part of the *y*-polarized absorbance is most likely borrowed from the strong *E* band by vibronic coupling. In addition, out-of-plane *x*-polarized transitions to states like 2 $^1B_1$ and 3 $^1B_1$ (Table 1) are predicted to contribute to the intensity of this band.

Band *C* was assigned by Gleiter et al. [3] to a π-π* transition described by the promotion corresponding to $5b_1(\pi) \rightarrow 3a_2(\pi^*)$. But the large shifts of this band observed when replacing sulfur by selenium were not well described by their calculations. The present results indicate that several transitions may contribute to this absorbance band.

Assignment of the long axis-polarized band *D* with a maximum at 37,400 cm^{-1} (267 nm) is difficult. No *z*-polarized absorbance is predicted in the region between bands *B* and *E*. In fact, no $^1A_1$ states are calculated between 2 $^1A_1$ at 26,700 cm^{-1} and 3 $^1A_1$ at 47,700 cm^{-1} (375 and 210 nm). More advanced calculations including doubly or multiply excited electronic configurations might predict the "missing $^1A_1$ state". In particular, inclusion of the doubly excited configuration derived by promotion of two electrons from $11b_2(n)$ to $6b_1(\pi^*)$ might lead to the prediction of an $^1A_1$ state in the region of band *D*. It is also possible that part of the observed absorbance *D* is due to one or more of the $^1A_2$, $^1B_1$, and $^1B_2$ states predicted in this region (Table 1) gaining *z*-polarized intensity by vibronic coupling with strong transitions to $^1A_1$ states. Perhaps band *D* borrows intensity from transitions to states outside the experimentally investigated region, such as 4 $^1A_1$ and 5 $^1A_1$ predicted at 48,500 and 50,000 cm^{-1} (206 and 200 nm). The onset of *z*-polarized absorbance due to such $^1A_1$ states seems to overlap the high-wavenumber edge of band *D* (Fig. 2 (top)).

Gleiter et al. [3] noticed that band *D* shows a considerable blue shift when changing to a solvent with larger polarity (negative solvatochromism), indicating the assignment of an n–π^* or n–σ* transition. They suggested transitions corresponding to $11b_2(n) \rightarrow 3a_2(\pi^*)$ and $11b_2(n) \rightarrow 18a_1(\sigma^*)$. Such promotions contribute to the transitions presently computed in this spectral region. But in any case, elucidation of the origin of band *D* requires the application of more advanced theoretical models.

We have here discussed the observed electronic transitions of DTT with reference to the results of the TD–CAM-B3LYP/AUG-cc-pVTZ calculation. These results are very similar to those obtained with larger basis sets, such as AUG-cc-pVQZ and AUG-cc-pV5Z (S5, S6), and also to those obtained with TD–ωB97XD/AUG-cc-pVTZ (S8). However, TD–CAM-B3LYP/6-311++G(3df,3pd) and TD–LC-ωPBE/AUG-cc-pVTZ predict a more or less deviating distribution of the *y*-polarized intensity (S2, S9). In particular, the latter procedure predicts a very different spectrum (S9), inconsistent with the experimental evidence.

5. Concluding remarks

The DTT chromophore is unusually complex for a molecule of this size (eight atoms). According to the present TD-DFT calculations, the complexity is partly due to the large number of virtual MOs predicted at low energy (Fig. 3). The inclusion of diffuse functions in the basis set has a profound influence on the predicted transitions, as illustrated by the comparison in S7 of results obtained with the bases cc-pVTZ and AUG-cc-pVTZ. This is not surprising in view of the recent results for TTF [1]. It is noteworthy that low-energy virtual orbitals of DTT show strong admixture of diffuse contributions, indicating mixed Rydberg-valence character; see the surface diagrams in Fig. 3 of the MOs $17a_1$, $12b_2$, $19a_1$, $13b_2$, and $7b_1$. Even the second lowest unoccupied MO, $17a_1$, is predicted to have pronounced non-valence character.

Similar TD-DFT calculations led to a satisfactory agreement with the observed near-UV polarization spectrum of TTF [1]. This may invite some confidence in the reliability of this level of theory in the study of DTT. We thus propose possible assignments of the observed spectral features to calculated electronic states, but more sophisticated theoretical investigations are necessary to elucidate the complexity of this chromophore. A full understanding may require the consideration of multiply excited electronic configurations and evaluation of multi-state multi-mode vibronic couplings [30–33].

CRediT authorship contribution statement

Kristin Visby: Methodology, Investigation, Formal analysis, Writing – review & editing. **Jens Spanget-Larsen:** Conceptualization, Methodology, Investigation, Resources, Formal analysis, Visualization, Writing – original draft, Writing – review & editing.

Declaration of Competing Interest

The authors declare that they have no known competing financial interests or personal relationships that could have appeared to influence the work reported in this paper.

Acknowledgements

We are grateful for useful discussions with Kristine Birklund Andersen and George Radziszewski and for assistance from Rita Buch in the laboratory.

Appendix A. Supplementary material

Supplementary data to this article can be found online at https://doi.org/10.1016/j.chemphys.2022.111574.

References

[1] P.W. Thulstrup, S.V. Hoffmann, N.C. Jones, J. Spanget-Larsen, Electronic transitions of tetrathiafulvalene oriented in polyethylene film. Near and vacuum UV synchrotron radiation polarization spectroscopy, Chem. Phys. Impact 2 (2021), 100009.

[2] F. Wudl, M.L. Kaplan, E.M. Engler, V.V. Patel, 2,2'-Bi-1,3-dithiolylidene (Tetrathiafulvalene, Ttf) and its radical cation salts, Inorg. Synth. 19 (1979) 27–34.

[3] J. Spanget-Larsen, R. Gleiter, M. Kobayashi, E.M. Engler, P. Shu, D.O. Cowan, The electronic structure of 1,3-dithiole-2-thione and Its selenium analogues. Photoelectron spectra and polarized electronic absorption spectra, J. Am. Chem. Soc. 99 (1977) 2855–2865.
[4] J. Michl, E.W. Thulstrup, Spectroscopy with Polarized Light: Solute Alignment by Photoselection, in Liquid Crystals, Polymers, and Membranes, VCH-Wiley, Deerfield Beach, FL, 1986, 1995.
[5] E.W. Thulstrup, J. Michl, Elementary Polarization Spectroscopy, Wiley-VCH, New York, Weinheim, 1989.
[6] F. Madsen, I. Terpager, K. Olskær, J. Spanget-Larsen, Ultraviolet-visible and infrared linear dichroism spectroscopy of 1,8-dihydroxy-9,10-anthraquinone aligned in stretched polyethylene, Chem. Phys. 165 (2-3) (1992) 351–360.
[7] A. Rodger, B. Nordén, Circular Dichroism and Linear Dichroism, Oxford University Press, UK, 1997.
[8] B. Nordén, A. Rodger, T. Dafforn, Linear Dichroism and Circular Dichroism: a Textbook on Polarized-Light Spectroscopy, RCS Publishing, Cambridge, UK, 2010.
[9] R. Pariser, R.G. Parr, A semi-empirical theory of the electronic spectra and electronic structure of complex unsaturated molecules, J. Chem. Phys. 21 (1953) 466–471.
[10] J.A. Pople, Electron interaction in unsaturated hydrocarbons, Trans. Faraday Soc. (London) 49 (1953) 1375–1385.
[11] J. Fabian, A. Mehlhorn, R. Zahradnik, Semiempirical calculations on sulfur-containing heterocycles, J. Phys. Chem. 72 (1968) 3975–3985.
[12] M.E. Casida, Review: time-dependent density-functional theory for molecules and molecular solids, J. Mol. Struct. THEOCHEM 914 (2009) 3–18.
[13] C. Adamo, D. Jacquemin, The calculations of excited-state properties with Time-Dependent Density Functional Theory, Chem. Soc. Rev. 42 (3) (2013) 845–856.
[14] J.B. Foresman, Æ. Frisch, Exploring Chemistry with Electronic Structure Methods, third ed., Gaussian Inc, Wallingford CT, 2015.
[15] J. Fabian, E. Fanghänel, Die UV-S-absorptionen der 2H-l,3-dithiol-2-thione, J. Prakt. Chem. 36 (1967) 287–303.
[16] K.R.G. Devi, D.N. Sathyanarayana, E.M. Engler, Infrared Spectra of 1,3-Dithiole-3-thione and its Selenium Analogues - Frequency Assignment and Molecular Force Constants, J. Mol. Struct. 71 (1981) 1–15.
[17] Kh. Iqbal, N.L. Owen, The vibrational spectrum of 1,3-dithiol-2-thione, J. Mol. Struct. 71 (1981) 91–95.
[18] M.J. Frisch, G.W. Trucks, H.B. Schlegel, G.E. Scuseria, M.A. Robb, J.R. Cheeseman, G. Scalmani, V. Barone, G.A. Petersson, H. Nakatsuji, X. Li, M. Caricato, A.V. Marenich, J. Bloino, B.G. Janesko, R. Gomperts, B. Mennucci, H.P. Hratchian, J.V. Ortiz, A.F. Izmaylov, J.L. Sonnenberg, D. Williams-Young, F. Ding, F. Lipparini, F. Egidi, J. Goings, B. Peng, A. Petrone, T. Henderson, D. Ranasinghe, V.G. Zakrzewski, J. Gao, N. Rega, G. Zheng, W. Liang, M. Hada, M. Ehara, K. Toyota, R. Fukuda, J. Hasegawa, M. Ishida, T. Nakajima, Y. Honda, O. Kitao, H. Nakai, T. Vreven, K. Throssell, J.A. Montgomery, Jr., J.E. Peralta, F. Ogliaro, M.J. Bearpark, J. J. Heyd, E.N. Brothers, K.N. Kudin, V.N. Staroverov, T.A. Keith, R. Kobayashi, J. Normand, K. Raghavachari, A.P. Rendell, J.C. Burant, S.S. Iyengar, J. Tomasi, M. Cossi, J.M. Millam, M. Klene, C. Adamo, R. Cammi, J. W. Ochterski, R.L. Martin, K. Morokuma, O. Farkas, J.B. Foresman, D.J. Fox, Gaussian16, Revision A.03, Gaussian, Inc., Wallingford CT, 2016.
[19] T. Yanai, D. Tew, N.A. Handy, New hybrid exchange-correlation functional using the Coulomb-attenuating method (CAM-B3LYP), Chem. Phys. Lett. 393 (2004) 51–57.
[20] S. Grimme, Calculation of the electronic spectra of large molecules, Rev. Comp. Chem. 20 (2004) 153–218.
[21] D.D. Nguyen, N.C. Jones, S.V. Hoffmann, J. Spanget-Larsen, Vacuum UV polarization spectroscopy of *p*-terphenyl, J. Phys. Chem. A 122 (1) (2018) 184–191.
[22] D.D. Nguyen, N.C. Jones, S.V. Hoffmann, J. Spanget-Larsen, Electronic states of dibenzo-*p*-dioxin. A synchrotron radiation linear dichroism investigation, Chem. Phys. 519 (2019) 64–68.
[23] D.D. Nguyen, N.C. Jones, S.V. Hoffmann, J. Spanget-Larsen, UV synchrotron radiation linear dichroism spectroscopy of the antipsoriatic drug anthralin, PeerJ Phys. Chem. 1 (2019), e5.
[24] T.H. Dunning Jr., Gaussian basis sets for use in correlated molecular calculations. I. The atoms boron through neon and hydrogen, J. Chem. Phys. 90 (2) (1989) 1007–1023.
[25] D.E. Woon, T.H. Dunning Jr., Gaussian-basis sets for use in correlated molecular calculations. 3. The atoms aluminum through argon, J. Chem. Phys. 98 (1993) 1358–1371.
[26] Y. Tawada, T. Tsuneda, S. Yanagisawa, T. Yanai, K. Hirao, A long-range-corrected time-dependent density functional theory, J. Chem. Phys. 120 (2004) 8425.
[27] O.A. Vydrov, J. Heyd, A. Krukau, G.E. Scuseria, Importance of short-range versus long-range Hartree-Fock exchange for the performance of hybrid density functionals, J. Chem. Phys. 125 (2006), 074106.
[28] J.-D. Chai, M. Head-Gordon, Long-range corrected hybrid density functionals with damped atom-atom dispersion corrections, Phys. Chem. Chem. Phys. 10 (2008) 6615–6620.
[29] R. Dennington, T.A. Keith, J.M. Millam, GaussView, Version 6.0.16 (Semichem Inc., Shawnee Mission, Kansas 66222, USA, 2016).
[30] G. Herzberg, E. Teller, Schwingungsstruktur der Elektronenübergänge bei mehratomigen Molekülen, Z. Physik. Chem. 21B (1933) 410–446.
[31] T. Azumi, K. Matsuzaki, Review: what does the term "Vibronic Coupling" Mean? Photochem. Photobiol. 25 (3) (1977) 315–326.
[32] F. Santoro, A. Lami, R. Improta, J. Bloino, V. Barone, Effective method for the computation of optical spectra of large molecules at finite temperature including the Duschinsky and Herzberg-Teller effect: The Q_x band of porphyrin as a case study, J. Chem. Phys. 128 (2008), 224311.
[33] F.-F. Kong, X.-J. Tian, Y. Zhang, Y.-J. Yu, S.-H. Jing, Y. Zhang, G.-J. Tian, Y. Luo, J.-L. Yang, Z.-C. Dong, J.G. Hou, Probing intramolecular vibronic coupling through vibronic-state imaging. Nat. Commun. 12 (2021) 1-8, and literature cited therein.